

Initial Study on the Impact of Speed Fluctuations on the Psychoacoustic Characteristics of a Distributed Propulsion System with Ducted Fans

Schade, S. ; Merino Martinez, R.; Ratei, P. ; Bartels, S. ; Jaron, R. ; Moreau, A

DOI

[10.2514/6.2024-3273](https://doi.org/10.2514/6.2024-3273)

Publication date

2024

Document Version

Final published version

Published in

30th AIAA/CEAS Aeroacoustics Conference (2024)

Citation (APA)

Schade, S., Merino Martinez, R., Ratei, P., Bartels, S., Jaron, R., & Moreau, A. (2024). Initial Study on the Impact of Speed Fluctuations on the Psychoacoustic Characteristics of a Distributed Propulsion System with Ducted Fans. In *30th AIAA/CEAS Aeroacoustics Conference (2024)* (30 ed.). Article AIAA 2024-3273 (30th AIAA/CEAS Aeroacoustics Conference, 2024). <https://doi.org/10.2514/6.2024-3273>

Important note

To cite this publication, please use the final published version (if applicable).
Please check the document version above.

Copyright

Other than for strictly personal use, it is not permitted to download, forward or distribute the text or part of it, without the consent of the author(s) and/or copyright holder(s), unless the work is under an open content license such as Creative Commons.

Takedown policy

Please contact us and provide details if you believe this document breaches copyrights.
We will remove access to the work immediately and investigate your claim.



Initial Study on the Impact of Speed Fluctuations on the Psychoacoustic Characteristics of a Distributed Propulsion System with Ducted Fans

S. Schade*

Bismarckstraße 101, 10625 Berlin, Germany

R. Merino-Martinez†

Delft University of Technology, Kluyverweg 1, 2629 HS Delft, the Netherlands

P. Ratei‡

Hein-Saß-Weg 22, 21229 Hamburg, Germany

S. Bartels§

Linder Höhe, 51147 Köln, Germany

R. Jaron¶ and A. Moreau||

Bismarckstraße 101, 10625 Berlin, Germany

New aircraft concepts with distributed propulsion systems are currently developed for urban and regional air mobility. Typically, these propulsion systems consist of a large amount of propulsors, such as ducted fans or propellers. As the emitted sound fields of individual propulsors may interact with each other, the noise emission is characterized by interference effects. These interactions change the psychoacoustic characteristics of distributed propulsion systems compared to conventional designs with two or four engines. Therefore, in this paper acoustic interactions due to rotational speed fluctuations are investigated for a distributed propulsion system equipped with 26 ducted, low-speed fans. Synthesized flyover sounds are generated using an analytical auralization process for different ranges of rotational speed fluctuations and the impact on noise immission as well as psychoacoustic sound quality metrics is assessed. Our study indicates that temporal fluctuations decrease with increased rotational speed fluctuations. Time signals are smoothed when speed fluctuations are applied, resulting in lower values for psychoacoustic loudness, tonality and fluctuation strength.

Nomenclature

bbn	broadband noise	mic	microphone
BPF	blade passing frequency	OGV	outer guide vane
C-Li, C-Ri	ith engine on the left/right canard wing	PropNoise	PropulsionNoise
CORAL	Aircraft engine noise auralization	RANS	Reynolds-averaged Navier Stokes
CRAFT	Co-/Contra Rotating Acoustic Fan Test	RSI	rotor-stator interaction
EPNL	effective perceived noise level [EPNdB]	SQAT	Sound Quality Analysis Toolbox
HRIR	Head Related Impulse Responses	SQM	sound quality metric

*Researcher, Institute of Propulsion Technology, stephen.schade@dlr.de

†Assistant professor, Aircraft Noise and Climate Effects section, Faculty of Aerospace Engineering

‡Researcher, Institute of System Architectures in Aeronautics

§Researcher, Institute of Aerospace Medicine

¶Deputy head of department, Institute of Propulsion Technology

|| Researcher, Institute of Propulsion Technology

TE	trailing edge	$max(PNLT(t))$	maximum tone corrected perceived noise level [dB]
UAM	urban air mobility	$M_{ax, in}$	inflow axial Mach number
VIOLIN	Virtual acoustic flyover simulation	M_{flight}	flight Mach number
VTOL	vertical take-off and landing	$M_{rel, tip}$	relative rotor tip Mach number
W- L_i , W- R_i	i th engine on the left/right main wing	N	rotational speed [rpm]
ΔN	rotational speed fluctuation [%]	n	relative rotational speed [%]
Δt	time step [s]	N_5	loudness [sone]
FS_5	fluctuation strength [vacil]	PA_5	psychoacoustic annoyance
i_{rotor}	rotor incidence angle [deg]	PR	pressure ratio
K_5	tonality [t.u.]	R_5	roughness [asper]
L_p, SPL	sound pressure level [dB]	S_5	sharpness [acum]
L_w	sound power level [dB]	η_{ise}	isentropic efficiency
\dot{m}	mass flow [kg/s]	μ	average
$max(L_p(t))$	maximum sound pressure level [dB]	σ	standard deviation

I. Introduction

So far, aircraft are usually powered by only a few engines, typically two or four. However, as part of current aviation research, distributed, electrified propulsion systems are developed to power a new generation of aircraft (e.g. air taxis for urban air mobility, UAM). These distributed propulsion systems might consist of a large number of propulsors. Consequently, the noise impact of these distributed propulsion systems is the result of the sum of the noise emissions of the individual propulsors. Therefore, acoustic interactions between the emitted sound fields are an essential characteristic of the noise emission of distributed propulsion systems [1, 2]. In addition, the number and installation position of the propulsors affect the noise emission, e.g. due to interference, modulation, and shielding effects. As a result, the noise emission will differ from conventional aircraft. The noise perception and annoyance of distributed propulsion systems is likely to also deviate from those of conventional aircraft and to depend on psychoacoustic factors [3] as it has already been discussed for smaller UAM vehicles/drones [4, 5]. These effects may become particularly relevant with a larger number of propulsors. In addition, for air taxis the same can be assumed as for drones, i.e. due to the lower flight altitudes and the closer distances between vehicle and observer and the resulting reduced impact of atmospheric absorption, the high-frequency noise and sharpness are crucial for the perception of UAM noise [4, 6]. In sum, noise perception is expected to be a key factor for the UAM acceptance of society [7].

Regarding the aerodynamic and aeroacoustic interactions between distributed propellers, several studies, mainly conducted using drones, are already available in literature [4, 5]. Pascioni and Rizzi [1] concluded that the initial angular position for each propeller significantly affect the radiation characteristics of a distributed propulsion system. Guérin and Tormen [2] confirmed that acoustic interferences resulting from different angular propeller positions and thus different phase relations remarkably change the tonal noise directivity of the distributed propulsion system. Bernardini et al. [8] investigated the aeroacoustic interactions between propellers based on their relative distance to each other.

However, acoustic interactions between distributed, low-speed ducted fans have not been extensively investigated yet. Therefore, in this paper, the impact of acoustic interactions on the psychoacoustic characteristics of a distributed propulsion system with ducted fans is investigated using the example of a UAM concept airplane. Distributed propulsion systems, in which each propulsor (e.g. propeller or fan) is powered by an individual motor, offer the opportunity to use the propulsors not only for thrust generation but also as a flight control system. As an example, rotational speed variations could intentionally be applied in order to achieve a certain flight condition. Moreover, also smaller random speed variations could occur if not all electric motors are perfectly synchronized. Speed variations or fluctuations lead to modulation effects with low modulation frequencies, which in turn result in tonal loudness fluctuations and thus affect the psychoacoustic characteristics of the propulsion system. This is discussed e.g. in [9] using the example of a drone and is investigated in this paper for a UAM vehicle powered by 26 distributed, ducted fans.

For this purpose, RANS-informed analytical noise predictions are applied to predict the noise emission of the fan stages, virtual flyover simulations are used to propagate the sound through the atmosphere, analytical noise syntheses

are performed to auralize the flyovers and acoustic as well as psychoacoustic sound quality metrics are calculated and compared. As frequency fluctuations particularly impact tonal noise, a low-broadband fan design that mainly radiates tonal noise is selected [10].

II. Tilt-duct vehicle and fan design

An UAM concept vehicle is designed as a basis for further high-fidelity disciplinary analysis and acoustic assessment. The choice of propulsion system is driven by the setup of the underlying research project. Herein, ducted fans and open rotors, are the two propulsion systems of interest for the acoustic assessment as they represent the vast design space for representative vehicle configurations in the field of urban and regional air mobility. Two vehicle concepts are developed, one with distributed, ducted fans and one with distributed rotors. As the focus of this paper is put on the psychoacoustic characteristics of low-speed fans, only the tilt-duct vehicle is presented in more detail.

In order to begin with the design of such vehicle concepts, a set of requirements is specified at the start. These top-level aircraft requirements aim to represent the urban and regional air mobility market segment and are comparable with existing real demonstration and production aircraft. The entry into service is assumed in 2030, the payload is 500 kg, a range of 150 – 200 km is assumed and the cruise speed is 200 – 250 km/h. The resulting vehicle concept is shown in an isometric perspective in Fig. 1(a).

The underlying methodology for vehicle design and sizing is based on handbook methods that have been derived from the state-of-the-art literature in the fields of aircraft and rotorcraft design with a special focus on the emerging methods for unconventional vehicles in urban and regional air mobility. The first application and demonstration of this methodology as part of an even larger simulation framework for vehicle and fleet design and assessment is presented in [11]. A complete documentation of the conceptual design methodology and tool implementation is available in [12].

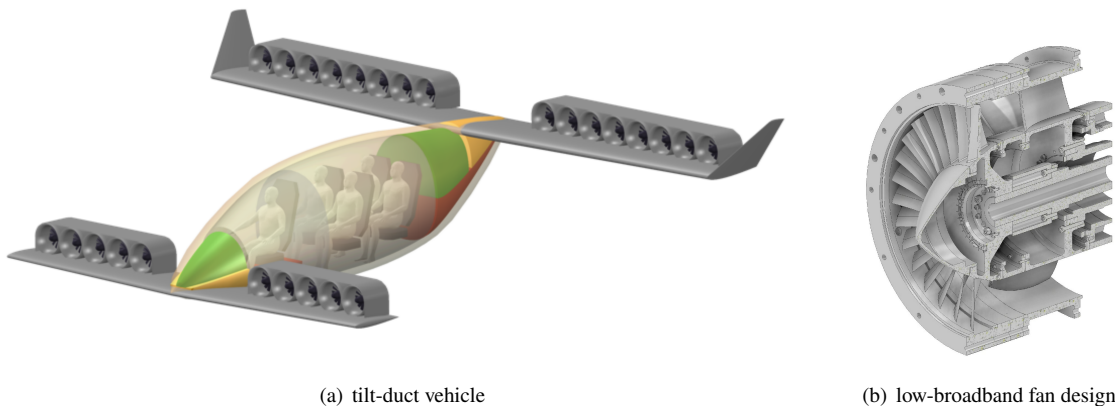


Fig. 1 Left: battery-electric vehicle concept as a basis for further high-fidelity disciplinary analysis and acoustic assessment; right: low-speed, ducted fan design.

The distributed propulsion system of the tilt-duct vehicle is equipped with 26 low-speed, ducted fan stages, where 10 fans are installed on the canard wing and 16 on the main wing. Each fan has a diameter of 0.45 m. Regarding the fan design, three different rotor-stator fan stages are available. The aerodynamic design of these fans and their acoustic characteristics are evaluated in [10]. Since rotational speed fluctuations mainly impact tonal noise, a low-broadband fan design, visualized in Fig. 1(b), is chosen for the noise studies presented in this paper. The low-broadband fan is a low-count OGV (outer guide vane) fan design meaning that fewer stator vanes (10) than rotor blades (31) are considered. Due to the low number of stator vanes, the broadband noise is reduced. Thus, the noise radiation is dominated by tonal noise which makes the fan particularly suitable for investigating rotational speed fluctuations. The operating conditions and performance of the low-broadband fan are summarized in Tab. 1, where N is the rotational speed, \dot{m} is the mass flow, i_{rotor} is the rotor incidence angle, $M_{\text{ax, in}}$ is the axial inflow Mach number, $M_{\text{rel, tip}}$ is the relative rotor tip Mach number, PR is the fan pressure ratio and η_{ise} is the fan isentropic efficiency.

The fan was initially developed for experimental testing in the CRAFT (Co-/Contra Rotating Acoustic Fan Test) facility [13, 14]. In the CRAFT test facility, ducted fan stages with representative conditions (e.g. rotor tip Mach number and fan pressure ratio) for urban air mobility engines can be experimentally examined.

Table 1 Operating conditions and performance of the low-broadband fan when mounted on the tilt-duct vehicle.

	N [rpm]	n [%]	\dot{m} [kg/s]	i_{rotor} [deg]	$M_{\text{ax, in}}$ [-]	$M_{\text{rel, tip}}$ [-]	PR [-]	η_{ise} [%]
Cruise	3375	100	5.25	2	0.11	0.26	1.021	90.0
Design	4500	133	6.98	2	0.14	0.31	1.038	90.5

III. Auralization framework

Auralization allows us to make acoustic results audible. The resulting time signals and audio files can be used for psychoacoustic studies, such as the assessment of psychoacoustic sound quality metrics or the execution of listening tests. The acoustic and psychoacoustic analysis of the tilt-duct distributed propulsion system is provided on the basis of an analytical process consisting of (1) a RANS-informed analytical noise prediction (see Sec. III.A), (2) virtual flyover simulation (see Sec. III.B), (3) sound synthesis (see Sec. III.C) and (4) psychoacoustic sound quality assessment (see Sec. III.D).

A. RANS-informed analytical noise prediction

The noise emission is determined using the in-house tool PropNoise (Propulsion Noise) [15, 16]. PropNoise is used to provide a RANS-informed analytical noise prediction [16]. Thus, 3D steady-state RANS simulations are performed for the low-broadband fan operated at Design conditions. Based on the RANS simulations, radial distributions of all necessary aerodynamic quantities (e.g. velocity distributions) are extracted. These radial distributions serve as an input for the acoustic module of PropNoise. The acoustic module relies on a radial strip approach to calculate the acoustic source terms which are then radially integrated to obtain the in-duct modal sound pressure amplitudes [15]. Based on the amplitudes the acoustic modal power is calculated. Afterwards, the propagation of sound through the duct segments as well as the radiation of sound from the inlet and outlet planes of the fan stage are determined. As an output, the directivity patterns are provided on a spherical surface of a specified radius parameterized by the polar radiation angle.

A detailed description of the RANS-informed noise prediction method with PropNoise can be obtained from [16]. In addition, the setup for the RANS simulations as well as the results of the RANS-informed noise prediction for the low-broadband fan are described in [10].

B. Virtual flyover simulation

The modal directivity patterns obtained from RANS-informed noise prediction serve as an input for the in-house tool VIOLIN (Virtual acoustic flyover simulation) [17, 18]. VIOLIN uses a frequency-domain approach to determine the noise immission. A virtual flyover simulation is performed and the noise is propagated through the atmosphere to one or several observer positions on the ground. VIOLIN accounts for the Doppler frequency shift, the atmospheric absorption [19], the impact of atmospheric turbulence on amplitude as well as phase relations [20, 21] and the attenuation as well as reflection of the sound waves on the ground [22, 23]. The outputs from VIOLIN are frequency- and time-dependent sound pressures at the selected microphone position.

The trajectory segment for the virtual flyover simulation is selected according to the EASA specifications for VTOL (vertical take-off and landing) aircraft powered by tilting rotors [24]. For the acoustic certification applicable to these aircraft, EASA defines four reference procedures: (1) take-off, (2) overflight, (3) approach and (4) hover. As the focus of this paper is to assess the impact of frequency fluctuation on noise perception, only the overflight procedure as well as the central microphone are considered initially. This reference procedure and the microphone position are visualized in Fig. 2. The flyover is performed for a simulation time of $t = 22$ s and the trajectory segment is discretized using a time step of $\Delta t = 0.015$ s. Design operating conditions (see Tab. 1) are applied to each fan stage and the flight Mach number is $M_{\text{flight}} = 0.17$. At design operating conditions, random distributions of rotational speed fluctuations are applied to the 26 fan stages. The fluctuations are static, which means that they do not change during flyover. Moreover, only the noise of the propulsion system is considered for the virtual flyover simulations. Thus, the assumption is made that the propulsion system is the dominant noise source. For all 26 fan stages, it is assumed that the initial angular positions of the rotor blades and the stator vanes are identical. Regarding the atmospheric conditions, the reference values are specified according to the EASA requirements [24]: the atmospheric pressure is set to 101325 Pa, the ambient air temperature is 25 °C, the relative humidity is 70 % and the wind speed is 0.5 m/s.

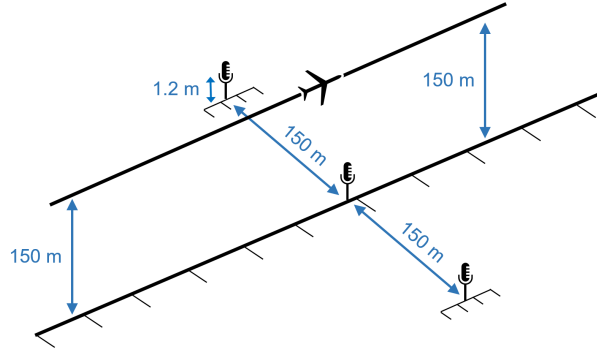


Fig. 2 Overflight reference procedure according to EASA specifications for VTOL aircraft powered by tilting rotors.

C. Noise synthesis

The spectrograms determined with VIOLIN represent the time- and frequency-dependent sound pressure levels at the specified observer positions (e.g. the central microphone according to Fig. 2). This is the input for the in-house tool CORAL (Aircraft engine noise auralization) [25].

Tonal and broadband noise sources are processed separately in CORAL: Tonal noise sources are considered as correlated. Thus, the spectrograms include phase information which means that complex sound pressure amplitudes are considered. From the tonal spectrograms, a time-varying sine signal is generated for each frequency in CORAL and all sine signals are then superimposed to obtain the overall time signal. By contrast, broadband noise sources are considered as uncorrelated. Consequently, no phase information is included in the spectrograms generated with VIOLIN. In CORAL, the broadband spectrograms are therefore provided with phase information by spectral multiplication with a white noise signal. Afterwards, the resulting time signals are generated using inverse short-time Fourier transformation.

CORAL provides a binaural noise synthesis and thus converts the spectrograms into one-dimensional time series for the left and right ear, respectively. In binaural sound synthesis, monaural time signals can be made stereo by filtering them with Head Related Impulse Responses (HRIRs). For this, a far-field HRIR data set, measured by Bernschütz [26], is considered. The audio files are then saved as Waveform Audio (.wav) files.

In [25] a validation of the sound synthesis is performed on the example of the A320 aircraft DLR ATRA, which is equipped with two V2500 engines.

D. Sound quality analysis

Sound Quality Metrics (SQMs) describe the subjective perception of sound by human hearing, unlike the sound pressure level metric, which quantifies the purely physical magnitude of sound based on the pressure fluctuations. Previous studies [27, 28] showed that these metrics capture the auditory behavior of the human ear in a better way than conventional sound metrics typically employed in noise assessments. The five most commonly-used SQMs [29] are:

- Loudness (N_5): Subjective perception of sound magnitude corresponding to the overall sound intensity [30].
- Tonality (K_5): Measurement of the perceived strength of unmasked tonal energy within a complex sound [31].
- Sharpness (S_5): Representation of the high-frequency sound content [32].
- Roughness (R_5): Hearing sensation caused by sounds with modulation frequencies between 15 Hz and 300 Hz [33].
- Fluctuation strength (FS_5): Assessment of slow fluctuations in loudness with modulation frequencies up to 20 Hz, with maximum sensitivity for modulation frequencies around 4 Hz [34].

These five SQMs were calculated for each audio file and the 5% percentile values (representing the value of each SQM exceeded 5% of the total recording time) are, henceforth, considered. These 5% percentile values were then combined into a single global psychoacoustic annoyance (PA_5) metric following the model outlined by Di *et al.* [35].

All the SQMs, as well as the EPNL and PA_5 metrics, were computed using the open-source MATLAB toolbox SQAT (Sound Quality Analysis Toolbox) v1.1 [29, 36]. The GitHub repository of the toolbox, including explanations of the implementations of each SQM as well as validations, can be found in [37].

IV. Results

In this section, the results of the analytical auralization process are evaluated. In Sec. IV.A the noise emission is analyzed, in Sec. IV.B the noise immission at the central microphone is assessed, and in Sec. IV.C the psychoacoustic sound quality metrics are evaluated. Selected audio files are available open-access in a *Zenodo* repository [38].

A. Noise emission

Figure 3(a) shows the 1/3 octave band frequency spectrum of the low-broadband fan at Design conditions. As this fan stage is equipped with only 10 stator vanes, the broadband component of the rotor-stator interaction (RSI) noise source is reduced. The reason is that the broadband RSI noise is proportional to the number of stator vanes. Thus, the lower the number of stator vanes the lower the broadband RSI noise levels. As a result, the noise emission of this fan is dominated by tonal noise. In particular, the fan tones at the first and second blade passing frequency (BPF) clearly dominate the frequency spectrum. Since the fan has 31 rotor blades and the rotational speed in $N = 4500$ rpm, the first BPF tone occurs at 2325 Hz. As frequency fluctuations especially affect tonal noise, this fan is well-suited to investigate the impact of rotational speed fluctuations on the psychoacoustic characteristics of a distributed propulsion system.

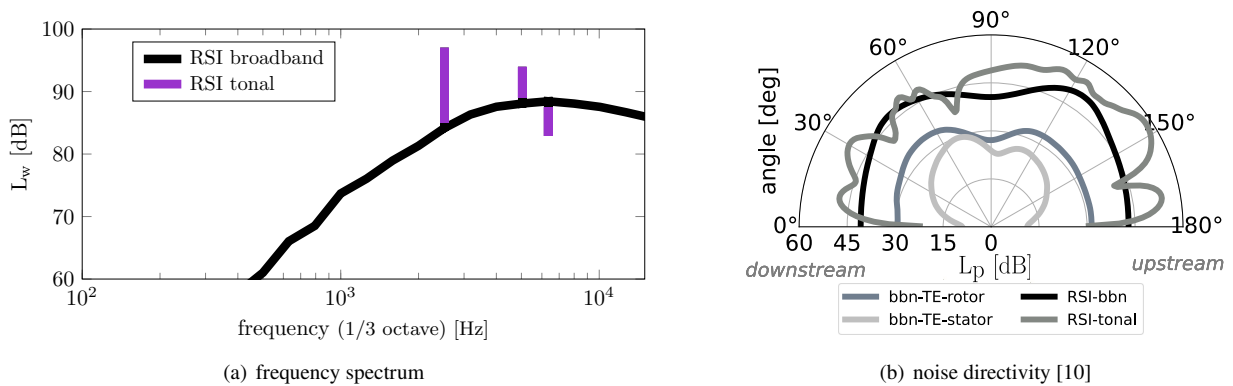


Fig. 3 Frequency spectrum and noise directivity pattern of the low-broadband fan operated at Design conditions obtained from RANS-informed noise prediction with PropNoise.

In order to illustrate the noise radiation characteristics of the fan, Fig. 3(b) shows the respective noise directivity for tonal and broadband RSI noise as well as trailing edge (TE) noise at Design conditions. For upstream noise radiation (see radiation angles between 90 deg and 180 deg in Fig. 3(b)), tonal RSI noise is the dominant noise source. Downstream, on the other hand, tonal noise is reduced so that the tonal RSI noise levels are approximately similar compared to the broadband levels for radiations angles between 0 deg and 80 deg. The acoustic effect employed to decrease the downstream tonal noise levels is explained and evaluated in [10].

As an intermediate summary, Tab. 2 outlines the upstream and downstream radiated tonal ($L_{w, \text{tonal}}$), broadband ($L_{w, \text{broadband}}$), and overall ($L_{w, \text{overall}}$) sound power levels. The sound power levels are obtained from the radiation module of PropNoise and are based on RANS-informed noise prediction as described in Sec. III.A. Whereas the radiated broadband sound power levels are approximately similar upstream and downstream, the tonal noise levels are remarkably lower downstream (92.9 dB) compared to upstream (97.6 dB). In addition, downstream, the tonal sound power level is slightly lower than the broadband level. The reduction in tonal noise is also reflected in the overall sound power levels: The dominant noise radiation direction is upstream with an overall sound power level of 99.4 dB. Downstream, the radiated overall sound power level is approximately 3 dB lower.

Table 2 Radiated tonal, broadband, and overall sound power levels for the low-broadband fan at Design conditions obtained from RANS-informed noise prediction with PropNoise.

	$L_{w, \text{tonal}}$ [dB]	$L_{w, \text{broadband}}$ [dB]	$L_{w, \text{overall}}$ [dB]
upstream	97.6	94.4	99.4
downstream	92.9	93.8	96.6

B. Noise immission

For the subsequent analysis, rotational speed fluctuations are applied to the distributed propulsion system equipped with 26 fan stages. Besides the ideal case, without any speed fluctuation, five ranges of speed fluctuation ΔN are considered: $\pm 0.25\%$, $\pm 0.5\%$, $\pm 1.0\%$, $\pm 2.0\%$, and $\pm 4.0\%$. The speed fluctuations are determined prior to the auralization process and are randomly distributed over the 26 fan stages. Thereby, the nominal rotational speed is the Design speed $N = 4500$ rpm as listed in Tab. 1. For the case $\Delta N = \pm 1.0\%$, ten random distributions are considered in order to assess the variability of the results.

Figure 4(a) shows the time-dependent pressure amplitudes at the central microphone of the overflight reference procedure for different ΔN . The sound pressure amplitudes are normalized to 90 dB and the dashed line indicates the time at which the microphone is passed.

Regarding the ideal case, the characteristic shape of the time signal mainly results from the impact of ground reflection, especially on tonal noise. As the microphone is positioned at a height of 1.2 m, interferences occur from the complex superposition of the direct and the reflected sound waves reaching the microphone. In particular, due to the spanwise distribution of the fan stages, a different distance to the microphone is obtained for each engine at each time step. Therefore, as a result of the different distances, the emitted tonal frequencies from each engine experience different Doppler frequency shifts, and, thus, small frequency variations occur even for the ideal case without rotational speed fluctuations. Since tonal noise sources are treated as correlated, a complex superposition of the direct and reflected tonal sound waves is considered. This leads to interferences which are visible as amplitude fluctuations in the time signal. These fluctuations result from modulations with relatively low modulation frequencies. The amplitude fluctuations due to modulation are particularly pronounced before passing the microphone (see $\Delta N = \pm 0\%$ and $t = 2 - 6$ s in Fig. 4(a)). It seems plausible that modulations are particularly visible in the time signal before passing the microphone, as the fan stages emit tonal noise mainly upstream (see emission angles between 100 deg and 180 deg in Fig. 3(b)). After passing the microphone overhead, broadband noise sources tend to dominate the noise radiation of the fan stages (see emission angles between 30 deg and 80 deg in Fig. 3(b)), so that weaker interference effects due to modulation occur (see $\Delta N = \pm 0\%$ and $t = 12 - 16$ s in Fig. 4(a)). The reason is that broadband noise sources are assumed to be uncorrelated. Nevertheless, some temporal fluctuations still remain present. All in all, due to the amplitude fluctuations resulting from modulation, higher values for the sound quality metric fluctuation strength are expected.

Compared to the impact of ground reflection, it is observed that atmospheric turbulence has only a minor impact on the time signals. This is reasonable, as almost ideal weather conditions (e.g. very low wind speed) are considered, as required for the acoustic certification.

Both the impact of ground reflection as well as atmospheric turbulence on the time signals as described above is additionally visualized in Fig. 8 in Appendix B. For Fig. 8, the advantage of analytical modeling is used that individual effects can be selectively evaluated. Accordingly, either the atmospheric turbulence or the ground reflection is switched off in order to be able to examine the respective influence of the effect on the time signal.

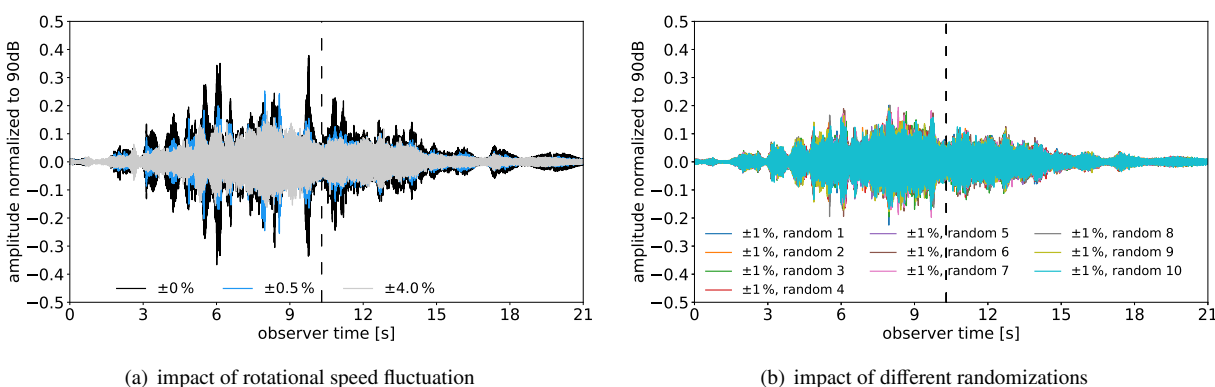


Fig. 4 Normalized sound pressure amplitudes at the central microphone.

Regarding the impact of rotational speed fluctuations on the time signals, it becomes obvious that temporal fluctuations in pressure amplitude decrease with increasing ΔN (see curves for $\pm 0.5\%$ and $\pm 4\%$ in Fig. 4(a)). Thus, it seems that the time signals are smoothed due to the rotational speed fluctuations. In addition, if rotational speed fluctuations are applied, the maximum sound pressure amplitude is also reduced. This reduction in sound pressure

amplitude is also reflected in the maximum sound pressure levels $\max(L_p(t))$ which are listed in Tab. 3. Note that the time signals are interpolated to a time step of $\Delta t = 0.5$ s prior to the calculation of $\max(L_p(t))$. This is done to ensure better comparability between $\max(L_p(t))$ and EPNL values, as a time step of $\Delta t = 0.5$ s is required for the EPNL metric [39]. Even for small values of ΔN (e.g. $\pm 0.5\%$), the maximum sound pressure level is reduced significantly compared to the ideal case with identical rotational speeds applied to each fan stage. The trend observed for the $\max(L_p(t))$ values is also reflected in the maximum tone-corrected perceived noise levels $\max(\text{PNLT}(t))$ and the effective perceived noise levels (EPNL) (see Tab. 3).

Since one random distribution of rotational speed fluctuation is generated once for each considered interval ($\pm 0.5\%$, $\pm 1.0\%$, $\pm 2.0\%$ and $\pm 4.0\%$), the question arises regarding the influence that this random distribution has on the results. Therefore, ten random distributions of speed fluctuation are generated within the interval $\Delta N = \pm 1.0\%$ and applied to the 26 fan stages. The resulting time signals are compared in Fig. 4(b). It is shown that the choice of the random distributions of speed fluctuation only slightly affects the time signals. Moreover, $\max(L_p(t))$, $\max(\text{PNLT}(t))$ and EPNL are averaged over ten random distributions and the standard deviations are calculated. The averages μ and standard deviations σ are listed in the last row of Tab. 3.

Table 3 Comparison between $\max(L_p(t))$, $\max(\text{PNLT}(t))$, and EPNL at the central microphone of the overflight reference procedure. Design operating conditions are considered. The last row indicates the statistical values (average μ and standard deviation σ) for $\Delta N = \pm 1.0\%$.

ΔN	$\max(L_p(t))$, [dB]	$\max(\text{PNLT}(t))$, [PNLTdB]	EPNL, [EPNdB]
$\pm 0\%$	76.4	92.7	85.7
$\pm 0.5\%$	68.9	85.7	81.3
$\pm 1.0\%$	66.9	84.3	80.0
$\pm 2\%$	67.5	84.5	80.7
$\pm 4\%$	65.6	83.7	80.3
$\pm 1.0\%$, 10 random distributions	$\mu = 66.9, \sigma = 0.66$	$\mu = 84.2, \sigma = 0.89$	$\mu = 79.9, \sigma = 0.40$

In order to better compare the time signals of the virtual flyover simulations performed with distributed low-speed fans, a reference time signal is shown in Fig. 5(a). The reference signal is obtained from a virtual flyover with two turbofan engines that could be used in an A320-like aircraft. A realistic take-off trajectory, which is described in [18], is used for the virtual flyover simulation. The noise sources are predicted analytically using PropNoise and the following sources are considered: buzz-saw noise, jet noise, and RSI noise (tonal and broadband). Identical weather conditions are applied as for the flyover simulation with distributed low-speed fans. Note that the scale of the y-axis is changed and that the amplitudes are normalized to 110 dB instead of 90 dB as the turbofan engine generates remarkably higher sound levels compared to the low-speed fans.

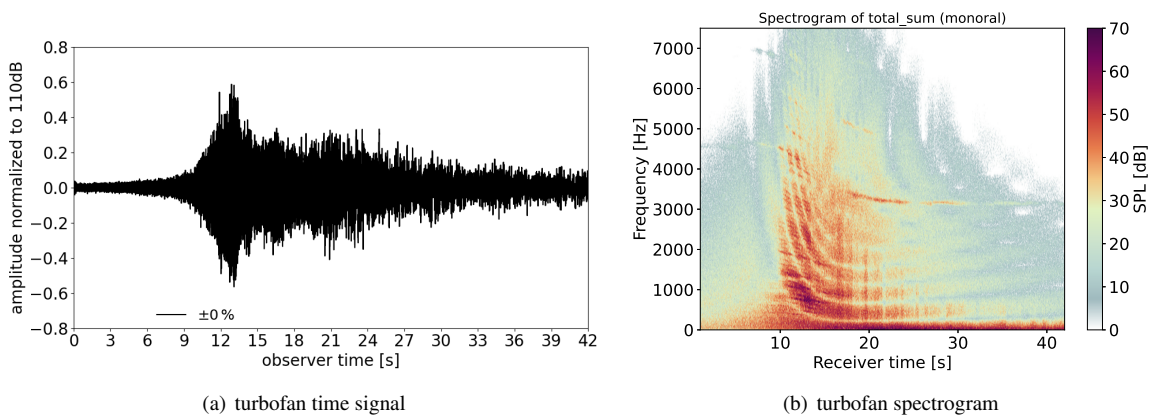


Fig. 5 Virtual reference flyover with two turbofan engines at Take-off.

To examine both temporal structures and spectral patterns, Fig. 6 shows the spectrograms for the central microphone

of the overflight reference procedure for different rotational speed variation intervals. To simplify the visualization, the monaural spectrograms are provided, although the audio files are, in fact, binaural. Please note that the dashed lines indicate the times at which the aircraft is located directly above the microphone. The reference spectrogram obtained from the virtual flyover with two turbofan engines is shown in Fig. 5(b).

Independent of the choice of the propulsion system (turbofan or distributed low-speed fans), the spectrograms show vertical and U-shaped stripes. The vertical stripes result from acoustic interferences due to the modeled atmospheric turbulence, and the U-shaped stripes result from interferences due to the reflection of the sound waves on the ground. The ground is modeled as a flat and acoustically hard surface. Similar to the time signals, the influence of atmospheric turbulence and ground reflection is also selectively evaluated for the spectrograms and the results are additionally visualized in Fig. 8 in Appendix B.

The spectrograms shown in Fig. 6 clearly reflect the analyzed noise emission characteristics of the low-broadband fan stage. The fan tones are recognizable between 2000 Hz and 3000 Hz (first BPF), as well as between 4000 Hz and 5500 Hz (second harmonic). In addition, tonal noise is particularly dominant before passing the microphone (see $t = 0 - 11$ s). This is reasonable due to the aforementioned shape of the tonal noise directivity (see Fig. 3(b)).

Moreover, even for the ideal case without any speed fluctuations, the fan tones occur in narrow frequency bands and not at discrete frequencies. The reason is that 26 spanwise distributed fans are employed and, due to the spanwise fan distributions, different Doppler frequency shifts are observed. Therefore, the tones occurring at the harmonics of the blade passing frequency are clustered around narrow frequency bands. If random speed fluctuations are applied, the bandwidth of these tonal frequency bands enlarge, since the emitted frequencies not only experience a different Doppler shift but also randomly deviate from each other. This becomes particularly obvious for the case $\pm 4\%$, since the frequencies further separate from each other as the speed fluctuations increase. As a result, the narrow tonal frequency bands split into several discrete tones.

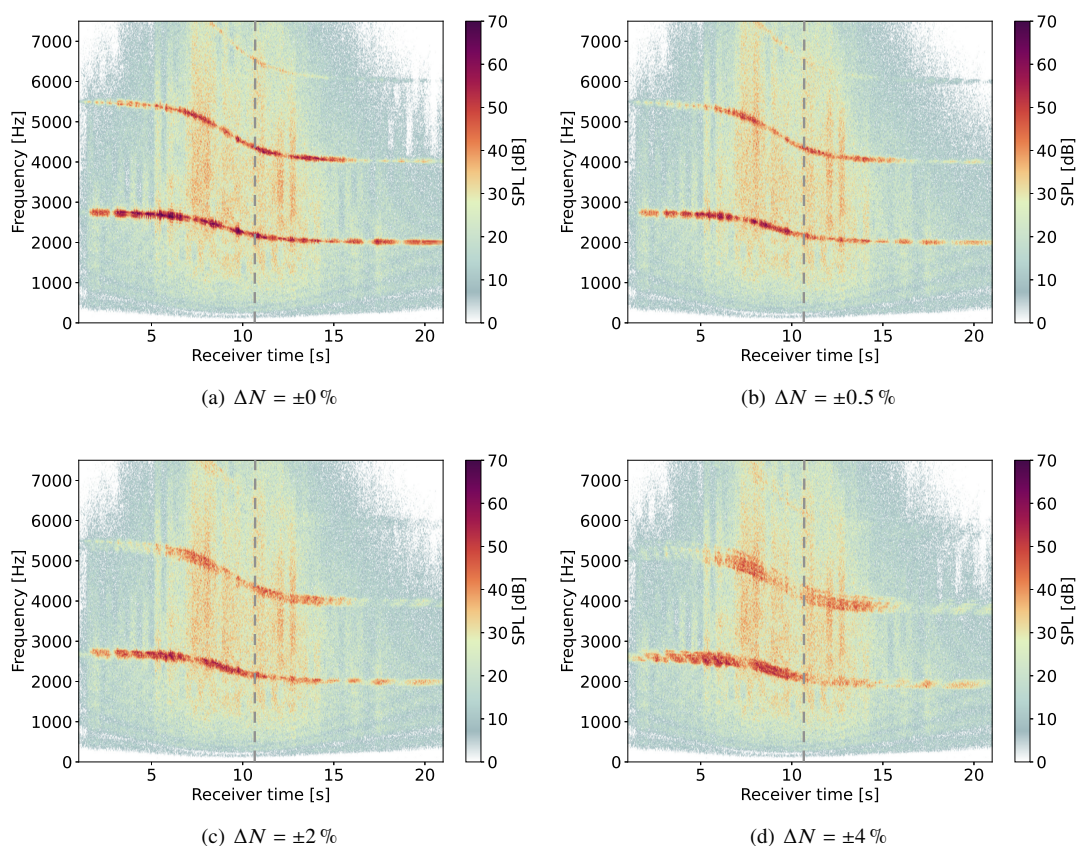


Fig. 6 Spectrograms at the central microphone of the overflight reference procedure. The fans are operated at Design conditions and different ranges of rotational speed fluctuations are applied.

C. Psychoacoustic parameters

An overview of the impact of ΔN on the values of the five different SQMs considered, as well as the psychoacoustic annoyance (PA) metric (see section III.D) is shown in Fig. 7. For comparison purposes, the values of the virtual reference flyover with two turbofan engines are also depicted. Note that for loudness and psychoacoustic annoyance the y-axes are plotted in logarithmic scale as large differences are observed between turbofan engines and low-speed fans. In addition, the variability of each SQM for the ten different randomizations evaluated for the case with $\Delta N = \pm 1.0\%$ are also denoted as an error bar.

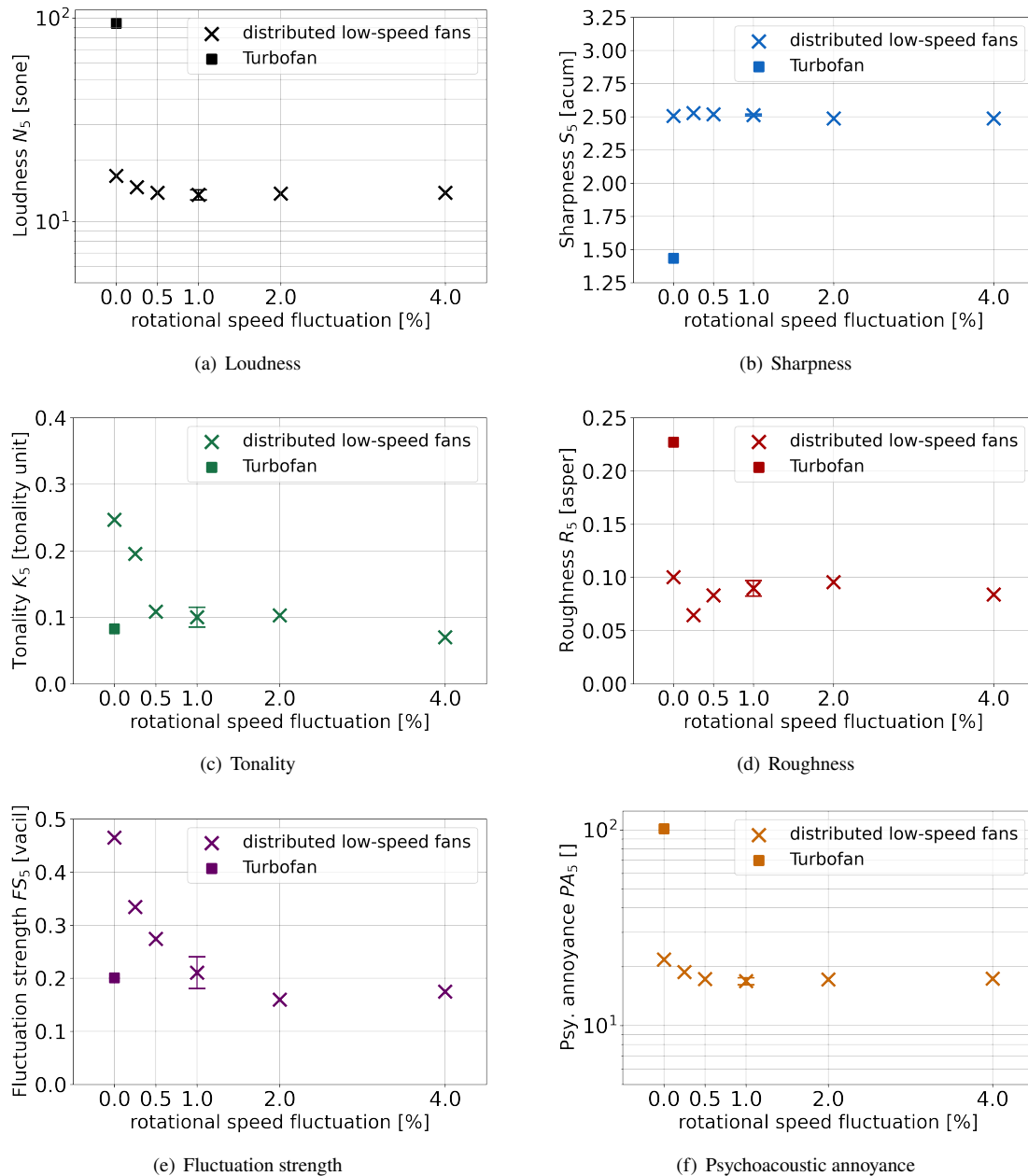


Fig. 7 Overview of the influence of the rotational speed fluctuations on the respective values of each SQM considered, as well as the psychoacoustic annoyance (PA). The SQM values for the virtual reference flyover with two turbofan engines are added for comparison purposes.

For the loudness metric (N_5 , see Fig. 7(a)), it can be observed that all the values corresponding to distributed low-speed fans are considerably below the reference value of the turbofan engines, as expected, due to its considerably

louder noise signature. It seems like increasing ΔN slightly decreases the loudness values, with the maximum reductions achieved around $\Delta N = \pm 1.0\%$. This reduction agrees with the reduction in pressure amplitudes aforementioned in Fig. 4(a).

The sharpness metric (S_5 , see Fig. 7(b)), on the other hand, remains almost constant (about 2.5 acum) for all ranges of ΔN , since the high-frequency content does not change significantly. Given the considerably smaller size of the low-speed fans, their noise signature has a stronger high-frequency content than the reference turbofan case (around 1.4 acum). Moreover, due to the relatively large amount of rotor blades (31) the tones occurring at the blade passing frequency and its harmonics are within the higher frequency range. Due to these reasons, the sharpness increases for the low-speed fans compared to the turbofan case.

The effect of the rotational speed fluctuations is quite noticeable for the tonality metric (K_5 , see Fig. 7(c)). In general, increasing ΔN leads to a considerable decrease in the observed tonality, with minimum values obtained for fluctuations around $\Delta N = \pm 4.0\%$. In that case, similar values as the reference turbofan case (0.09 t.u.) are reported. This reduction agrees with the enlargement of the tonal bandwidth (and hence lower tonality) as the rotational speed fluctuations increase aforementioned in Fig. 6.

The two metrics related to loudness modulations (roughness R_5 and fluctuation strength FS_5) present relatively low values for all cases, see Figs. 7(d) and 7(e). For roughness, the minimum value is obtained for $\Delta N = \pm 0.25\%$ around 0.06 asper, but the variation for other cases is not very pronounced. Overall, the roughness values are remarkably below the reference turbofan case (around 0.23 asper). Conversely, the fluctuation strength metric presents an almost monotonically decreasing behaviour with increasing ΔN . A minimum value of around 0.17 vacil is achieved for the case $\Delta N = \pm 2.0\%$, which is comparably similar to the reference turbofan case value (around 0.2 asper). The decrease in the fluctuation strength metric with increasing ΔN seems reasonable as it is observed that temporal fluctuations decrease and thus, the time signals are smoothed due to the speed fluctuations (see Fig. 4(a)).

Lastly, the global psychoacoustic annoyance metric (PA_5 , see Fig. 7(f)) presents a very similar trend as loudness, since that is the dominant metric influencing annoyance [29]. Overall, it seems that the minimum PA values are obtained for rotational speed fluctuations around $\pm 1.0\%$, whereas the maximum PA is reported for the ideal case without rotational speed fluctuations. As for the loudness, the reference case with two turbofan engines presents considerably higher values than the distributed low-speed fans, as expected.

Overall, the effect of the ten different randomizations considered for the case with $\Delta N = \pm 1.0\%$ has a negligible impact in the values of the SQMs. This conclusion is in line with the similar pressure amplitudes observed in Fig. 4(b).

V. Discussion and summary

In this paper, the impact of small, random speed fluctuations on the noise immission and psychoacoustic characteristics was investigated for a distributed propulsion system equipped with 26 low-speed, ducted fan stages. It was found that temporal fluctuations in sound pressure amplitude decrease with increasing speed fluctuations. As a consequence, the time signals are smoothed when speed fluctuations are applied. In addition, the results showed that when rotational speed fluctuations are considered, the maximum sound pressure level is reduced compared to the ideal case without any fluctuations. This trend is also reflected in the maximum as well as effective perceived noise levels.

A psychoacoustic analysis, evaluating different sound quality metrics (SQMs), confirmed the aforementioned noise reduction with increasing rotational speed fluctuations. The metrics of loudness, tonality, and fluctuation strength were particularly benefited by an increase in rotational speed fluctuations, providing an overall psychoacoustic annoyance reduction compared to the ideal case without speed fluctuations whilst sharpness and roughness did not change considerably. Nevertheless, the resulting beneficial effect of the increase of rotational speed fluctuations on psychoacoustic annoyance as predicted by a metric following the model outlined by Di *et al.* [35] needs to be replicated in upcoming listening tests with human subjects.

Compared to conventional turbofan engines, loudness was remarkably lower for the low-speed fans - as expected - because of the considerably higher sound pressure levels resulting at a simulated realistic take-off trajectory. Similarly, psychoacoustic annoyance was reduced for low-speed fans. This finding is not surprising since psychoacoustic annoyance is mostly influenced by loudness [3, 5]. However, this finding cannot be generalized to the conclusion that low-speed fans are generally less annoying than conventional turbofan engines. For a fair comparison, sound pressure levels need to be held constant between the different engine types. Besides loudness, sharpness and fluctuation strength have been shown to influence psychoacoustic annoyance (at least in studies on drones, e.g. [6]). Similarly to the present results on a high sharpness in low-speed fan sounds, increased sharpness values have already been reported for drone sounds [5] and, for the same reference sound pressure level, drone noise has been shown to be more annoying than conventional

aircraft noise [6]. Upcoming listening tests with human subjects will aim to address these open points and furthermore investigate the impact of personal and contextual effects, which are likely to be relevant not only for the psychoacoustic annoyance measured in the laboratory but also for the annoyance of the community [5].

Regarding the ideal case without any speed fluctuations, it should be noted that this is probably a theoretical case which is difficult or practically even impossible to achieve in reality. Since it is assumed that each fan is powered by an individual electric motor, a variety of potential reasons may lead to speed variations. For instance, some motors could be used to control and regulate the flight path of the aircraft. In this case, speed variations are used intentionally. In addition, the motors generally allow a certain tolerance when regulating the speeds, which means that the individual engines are not necessarily exactly synchronized. This may lead to small deviations regarding rotational speed.

For the investigation, the initial relative angular position is set identically between all rotor blades and all stator vanes. As investigated in [1, 2], this could lead to additional interference effects. However, for the stator vanes, it might be reasonable to assume that the angular position is identical, as the stator vanes do not rotate and are mounted in a fixed position during manufacturing. Regarding the rotor blades, the relative angular position would be expected to vary from engine to engine. Nevertheless, since a fan with 31 rotor blades is used for this study, the angles between neighboring blades are very small. Therefore, it is assumed that this effect is negligible.

In the present study, one microphone position of one certification trajectory is considered. In order to gain a more detailed understanding of the impact of speed variations on the psychoacoustic characteristics of distributed propulsion systems, further trajectories and microphone positions should be considered (e.g. as specified in the EASA guidelines [24]). For the present case, in which the microphone is positioned centrally under the trajectory, the modulation and interference effects may be particularly pronounced [2]. This should be additionally verified by analyzing the noise levels at lateral microphone positions. Moreover, in this study, the ground is modeled as a flat, acoustically hard surface. Thus, the sound waves are reflected by the ground but are not damped. Typically, in reality, one would expect that the ground not only reflects the sound waves but also provides a frequency-dependent attenuation. Due to a frequency-dependent attenuation, the analyzed amplitude fluctuations could possibly be mitigated. This should be analyzed in future studies using an impedance model for ground attenuation.

Acknowledgments

This publication is part of the project *Listen to the future* (with project number 20247) of the research program Veni 2022 (Domain Applied and Engineering Sciences) granted to Roberto Merino-Martinez which is (partly) financed by the Dutch Research Council (NWO).

A. Tilt-duct vehicle engine center positions

Table 4 Engine center coordinates relative to the airplane center position specified in the airplane reference frame.

engine	x [m]	y [m]	z [m]
C-L1	3.0	1.5	-0.5
C-L2	3.0	2.0	-0.5
C-L3	3.0	2.5	-0.5
C-L4	3.0	3.0	-0.5
C-L5	3.0	3.5	-0.5
C-R1	3.0	-1.5	-0.5
C-R2	3.0	-2.0	-0.5
C-R3	3.0	-2.5	-0.5
C-R4	3.0	-3.0	-0.5
C-R5	3.0	-3.5	-0.5
W-L1	-3.0	1.5	0.5
W-L2	-3.0	2.0	0.5
W-L3	-3.0	2.5	0.5
W-L4	-3.0	3.0	0.5
W-L5	-3.0	3.5	0.5
W-L6	-3.0	4.0	0.5
W-L7	-3.0	4.5	0.5
W-L8	-3.0	5.0	0.5
W-R1	-3.0	-1.5	0.5
W-R2	-3.0	-2.0	0.5
W-R3	-3.0	-2.5	0.5
W-R4	-3.0	-3.0	0.5
W-R5	-3.0	-3.5	0.5
W-R6	-3.0	-4.0	0.5
W-R7	-3.0	-4.5	0.5
W-R8	-3.0	-5.0	0.5

B. Impact of atmospheric turbulence and ground attenuation on time signals and spectrograms

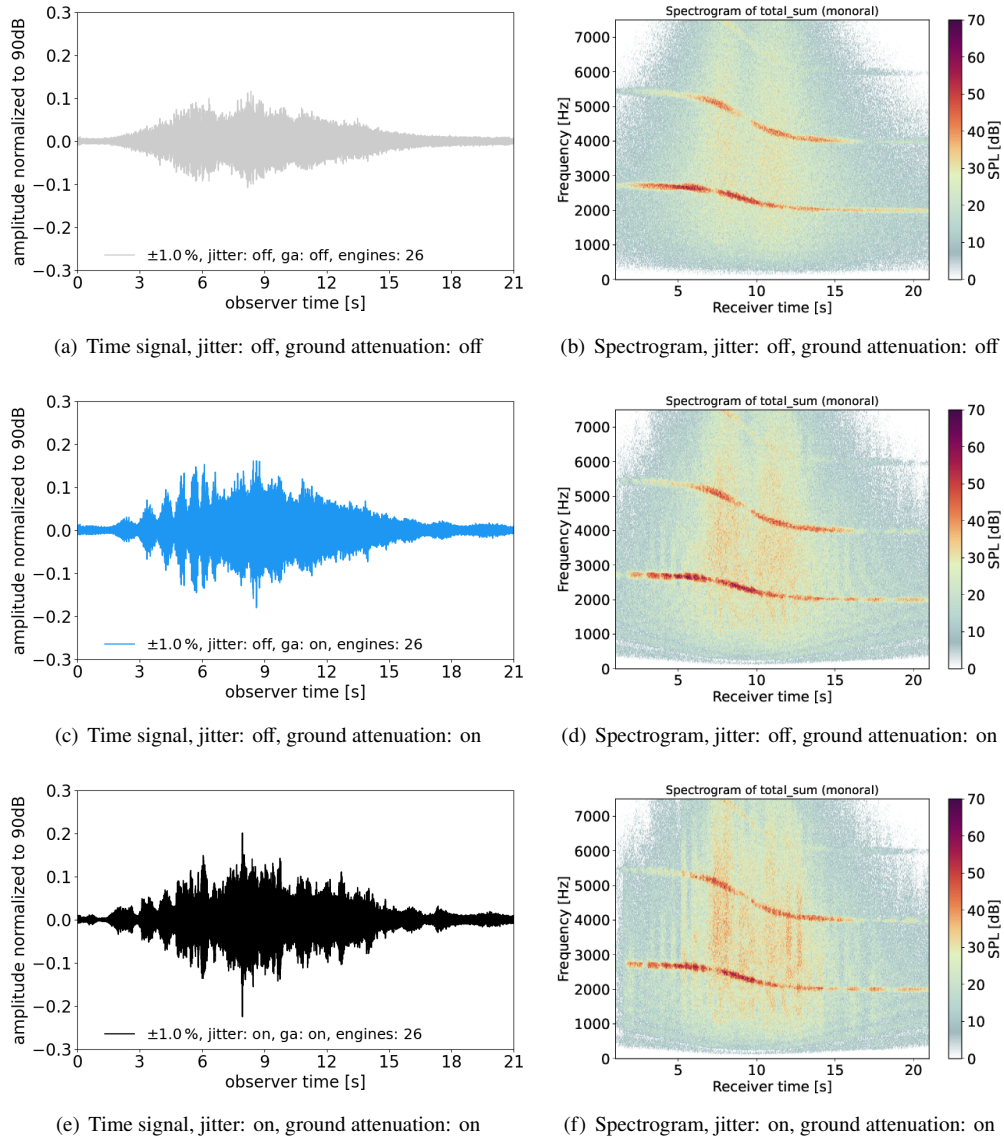


Fig. 8 Times signals left and spectrograms right.

References

- [1] Pascioni, K., and Rizzi, S. A., “Tonal Noise Prediction of a Distributed Propulsion Unmanned Aerial Vehicle,” *2018 AIAA/CEAS Aeroacoustics Conference*, 2018. <https://doi.org/10.2514/6.2018-2951>.
- [2] Guérin, S., and Tormen, D., “A contribution to the investigation of acoustic interferences in aircraft distributed propulsion,” *CEAS Aeronautical Journal*, Vol. 14, 2023, pp. 965–982. <https://doi.org/10.1007/s13272-023-00679-6>.
- [3] Boucher, M., Rafaelof, M., Begault, D., and et al., A. C., “A Psychoacoustic Test for Urban Air Mobility Vehicle Sound Quality,” *SAE Int. J. Adv. Curr. Prac. in Mobility*, Vol. 6, No. 2, 2024, pp. 972–985. <https://doi.org/10.4271/2023-01-1107>.
- [4] Torija, A. J., and Clark, C., “A Psychoacoustic Approach to Building Knowledge about Human Response to Noise of Unmanned Aerial Vehicles,” *International Journal of Environmental Research and Public Health*, Vol. 18, No. 2, 2021. <https://doi.org/10.3390/ijerph18020682>.
- [5] Lotinga, M. J. B., Ramos-Romero, C., Green, N., and Torija, A. J., “Noise from Unconventional Aircraft: A Review of Current Measurement Techniques, Psychoacoustics, Metrics and Regulation,” *Current Pollution Reports*, Vol. 9, No. 4, 2023. <https://doi.org/10.1007/s40726-023-00285-4>.
- [6] Gwak, D. Y., Han, D., and Lee, S., “Sound quality factors influencing annoyance from hovering UAV,” *Journal of Sound and Vibration*, Vol. 489, 2020. <https://doi.org/10.1016/j.jsv.2020.115651>.
- [7] Rizzi, S. A., Huff, D. L., Boyd, D. D., Bent, P., Henderson, B. S., Pascioni, K. A., Sargent, D. C., Josephson, D. L., Marsan, M., He, H., and Snider, R., “Urban Air Mobility Noise: Current Practice, Gaps, and Recommendations,” *NASA/TP-2020-5007433*, 2020.
- [8] Bernardini, G., Centracchio, F., Gennaretti, M., Iemma, U., Pasquali, C., Poggi, C., Rossetti, M., and Serafini, J., “Numerical Characterisation of the Aeroacoustic Signature of Propeller Arrays for Distributed Electric Propulsion,” *Applied Sciences*, Vol. 10, No. 8, 2020. <https://doi.org/10.3390/app10082643>.
- [9] Cabell, R., McSwain, R., and Grosveld, F., “Measured Noise from Small Unmanned Aerial Vehicles,” *NOISE-CON 2016*, 2016. URL <https://ntrs.nasa.gov/citations/20160010139>.
- [10] Schade, S., Jaron, R., Klähn, L., and Moreau, A., “Smart Blade Count Selection to Align Modal Propagation Angle with Stator Stagger Angle for Low-Noise Ducted Fan Designs,” *Aerospace*, Vol. 11, No. 4, 2024. <https://doi.org/10.3390/aerospace11040259>.
- [11] Prakasha, P. S., Ratei, P., Naeem, N., Nagel, B., and Bertram, O., “System of Systems Simulation driven Urban Air Mobility Vehicle Design,” *AIAA AVIATION 2021 FORUM*, 2021. <https://doi.org/10.2514/6.2021-3200>.
- [12] Ratei, P., “Development of a Vertical Take-Off and Landing Aircraft Design Tool for the Application in a System of Systems Simulation Framework,” Master thesis, Hamburg University of Applied Sciences (HAW Hamburg), Juni 2022. URL <https://elib.dlr.de/186947/>.
- [13] Tapken, U., Caldas, L., Meyer, R., Behn, M., Klähn, L., Jaron, R., and Rudolphi, A., “Fan test rig for detailed investigation of noise generation mechanisms due to inflow disturbances,” *AIAA AVIATION 2021 FORUM*, 2021. <https://doi.org/10.2514/6.2021-2314>.
- [14] Caldas, L., Kruck, S., Klähn, L., Rudolphi, A., Meyer, R., Enghardt, L., and Tapken, U., “Construction and Assessment of an Inflow-Control-Device for a Low-Speed Aeroacoustic Fan Rig,” *AIAA Journal*, Vol. 60, No. 9, 2022, pp. 1–14. <https://doi.org/10.2514/1.J061729>.
- [15] Moreau, A., “A unified analytical approach for the acoustic conceptual design of fans for modern aero-engines,” Dissertation, German Aerospace Center, Institute of Propulsion Technology, Berlin, Germany, 2017. <https://doi.org/10.14279/depositonce-5935>.
- [16] Jaron, R., “Aeroakustische Auslegung von Triebwerksfans mittels multidisziplinärer Optimierungen,” Dissertation, German Aerospace Center, Institute of Propulsion Technology, Berlin, Germany, 2018. <https://doi.org/10.14279/depositonce-7057>.
- [17] Dang, M., “Usability and maintainability of the software tools VIOLIN and CORAL,” Bachelor thesis, Baden-Württemberg Cooperative State University, 2022.
- [18] Prescher, A., “Mollierung der Schallausbreitung in einer inhomogenen Atmosphäre und ihr Einfluss auf binaural synthetisierten Überfluglärm,” Master thesis, Technical University of Berlin, 2023.
- [19] ISO 9613-1, “Attenuation of sound during propagation outdoors, Part 1: Calculation of the absorption of sound by the atmosphere,” No. ISO 9613-1, 1993. URL <https://www.iso.org/standard/17426.html>.
- [20] Rietdijk, F., Forssén, J., and Heutschi, K., “Generating Sequences of Acoustic Scintillations,” *Acta Acustica united with Acustica*, Vol. 103, No. 2, 2017, pp. 331–338. <https://doi.org/10.3813/AAA.919061>.
- [21] Prescher, A., Moreau, A., and Schade, S., “Model extension of random atmospheric inhomogeneities during sound propagation for engine noise auralization,” *Deutsche Luft- und Raumfahrtkongress - DLRK 2023*, Vol. conference proceedings, 2023.
- [22] Arbeitsgruppe Novellierung der AzB, “Anleitung zur Berechnung von Lärmschutzbereichen (AzB),” *Umweltbundesamt*, 2007.
- [23] Hornikx, M., “Ten questions concerning computational urban acoustics,” *Building and Environment*, Vol. 106, 2016, pp. 409–421. <https://doi.org/10.1016/j.buildenv.2016.06.028>.

- [24] EASA, “Environmental Protection Technical Specifications applicable to VTOL-capable aircraft powered by tilting rotors,” *consultation paper*, Vol. 1, 2023. URL <https://www.easa.europa.eu/en/document-library/product-certification-consultations/consultation-paper-environmental-protection-0>.
- [25] Moreau, A., Prescher, A., Schade, S., Dang, M., Jaron, R., and Guérin, S., “A framework to simulate and to auralize the sound emitted by aircraft engines,” *InterNoise conference 2023*, Vol. conference proceedings, 2023.
- [26] Bernschütz, B., “A Spherical Far Field HRIR/HRTF Compilation of the Neumann KU 100,” *Proceedings of the 39th DAGA*, 2013, pp. 592–595.
- [27] Merino-Martinez, R., Pieren, R., and Schäffer, B., “Holistic approach to wind turbine noise: From blade trailing–edge modifications to annoyance estimation,” *Renewable and Sustainable Energy Reviews*, Vol. 148, No. 111285, 2021, pp. 1–14. <https://doi.org/10.1016/j.rser.2021.111285>, URL <https://doi.org/10.1016/j.rser.2021.111285>.
- [28] Merino-Martinez, R., Pieren, R., Schäffer, B., and Simons, D. G., “Psychoacoustic model for predicting wind turbine noise annoyance,” *24th International Congress on Acoustics (ICA), October 24 – 28 2022, Gyeongju, South Korea*, 2022. URL https://www.researchgate.net/publication/364996997_Psychoacoustic_model_for_predicting_wind_turbine_noise_annoyance.
- [29] Greco, G. F., Merino-Martinez, R., Osses, A., and Langer, S. C., “SQAT: a MATLAB-based toolbox for quantitative sound quality analysis,” *52th International Congress and Exposition on Noise Control Engineering, August 20 – 23 2023, Chiba, Greater Tokyo, Japan*, International Institute of Noise Control Engineering (I-INCE), 2023. URL https://www.researchgate.net/publication/373334884_SQAT_a_MATLAB-based_toolbox_for_quantitative_sound_quality_analysis.
- [30] “ISO norm 532–1 – Acoustics – Method for calculating loudness – Zwicker method,” Tech. Rep. 1, International Organization for Standardization, 2017. URL <https://www.iso.org/obp/ui/#iso:std:iso:532:-1:ed-1:v2:en>.
- [31] Aures, W., “Berechnungsverfahren für den sensorischen Wohlklang beliebiger Schallsignale,” *Acta Acustica united with Acustica*, Vol. 59, No. 2, 1985, pp. 130–141.
- [32] von Bismark, G., “Sharpness as an attribute of the timbre of steady sounds,” *Acta Acustica united with Acustica*, Vol. 30, No. 3, 1974, pp. 159–172. URL <https://www.semanticscholar.org/paper/Sharpness-as-an-attribute-of-the-timbre-of-steady-Bismarck/9576a2a74bff46ee0cded25bfd9e4302b4fb0470>.
- [33] Daniel, P., and Webber, R., “Psychoacoustical Roughness: Implementation of an Optimized Model,” *Accustica – acta acustica*, Vol. 83, 1997, pp. 113–123. URL <https://www.ingentaconnect.com/contentone/dav/aaua/1997/00000083/00000001/art00020>.
- [34] Osses, A., García León, R., and Kohlrausch, A., “Modelling the sensation of fluctuation strength,” *22nd International Congress on Acoustics (ICA), September 5 – 9 2016, Buenos Aires, Argentina*, 2016. URL https://pure.tue.nl/ws/portalfiles/portal/52366479/Osses_Garcia_Kohlrausch_ICA2016_ID113.pdf.
- [35] Di, G.-Q., Chen, X.-W., Song, K., Zhou, B., and Pei, C.-M., “Improvement of Zwicker’s psychoacoustic annoyance model aiming at tonal noises,” *Applied Acoustics*, Vol. 105, 2016, pp. 164–170. <https://doi.org/10.1016/j.apacoust.2015.12.006>, URL <http://dx.doi.org/10.1016/j.apacoust.2015.12.006>.
- [36] Greco, G. F. and Merino-Martinez, R. and Osses, A., “SQAT: a sound quality analysis toolbox for MATLAB (version v1.1),” , May 2024. <https://doi.org/10.5281/zenodo.10580337>, URL <https://zenodo.org/records/10580337>, accessed in May 2024.
- [37] Greco, G. F. and Merino-Martinez, R. and Osses, A., “SQAT: a sound quality analysis toolbox for MATLAB,” , May 2023. URL <https://github.com/ggreco/sqat>, accessed in May 2023.
- [38] Schade, S., Merino-Martinez, R., Ratei, P., Bartels, S., Jaron, R., and Moreau, A., “Initial auralization of a distributed propulsion system equipped with 26 ducted low-speed fans,” *Zenodo*, 2024. <https://doi.org/10.5281/zenodo.11092740>.
- [39] “Federal Aviation Regulations, Part 36 (Appendix 2 to Section A36.4,” Tech. rep., Federal Aviation Administration, 800 Independence Avenue, SW, Washington, DC 20591, 2002. URL https://www.faa.gov/documentLibrary/media/Advisory_Circular/AC_36-4D.pdf.